Bioinspiration & Biomimetics

3D-printed hierarchical arrangements of actuators mimicking biological muscular architectures

To cite this article before publication: Corrado De Pascali *et al* 2023 *Bioinspir. Biomim.* in press https://doi.org/10.1088/1748-3190/acd159

IOP Publishing Bioinspiration & Biomimetics
Journal **XX** (XXXX) XXXXXX https://doi.org/XXXX/XXXX

3D-printed hierarchical arrangements of actuators mimicking biological muscular architectures

Corrado De Pascali[1,2,*], Stefano Palagi[2], Barbara Mazzolai[1,*]

[1] Bioinspired Soft Robotics Laboratory, Istituto Italiano di Tecnologia (IIT), Genova (GE), Italy

[2] The BioRobotics Institute, Scuola Superiore Sant'Anna, Pontedera (PI), Italy

∗Authors to whom any correspondence should be addressed.

E-mail: corrado.depascali@iit.it and barbara.mazzolai@iit.it

Abstract

Being able to imitate the sophisticated muscular architectures that characterize the animal kingdom in biomimetic machines would allow them to perform articulated movements with the same naturalness. In soft robotics, multiple actuation technologies have been developed to mimic the contraction of a single natural muscle, but a few of them can be implemented in complex architectures capable of diversifying deformations and forces. In this work, we present three different biomimetic muscle architectures, i.e., fusiform, parallel, and bipennate, which are based on hierarchical arrangements of multiple pneumatic actuators. These biomimetic architectures are monolithic structures composed of thirty-six pneumatic actuators each, directly 3D printed through low-cost printers and commercial materials without any assembly phase. The considerable number of actuators involved enabled the adoption and consequent comparison of two regulation strategies: one based on input modulation, commonly adopted in pneumatic systems, and one based on fiber recruitment, mimicking the regulation behavior of natural muscles. The straightforward realization through additive manufacturing processes of muscle architectures regulated by fiber recruitment strategies facilitates the development of articulated muscular systems for biomimetics machines increasingly similar to the natural ones.

Keywords: artificial muscles, soft pneumatic actuators, artificial muscular architecture, hierarchical muscle, fusiform muscle, bipennate muscle, parallel muscle, fiber recruitment, biomimetics, bioinspiration, soft robotics.

1) Introduction

Animals are capable of a wide variety of articulated movements, from the fast and powerful sprints performed by savannah felines to the tiny delicate deformations involved in human facial expressions. This broad range of movements is enabled by animals' muscular systems, composed of a variety of muscles that differ by quantity, size, shape, and hierarchical architectures. The single muscular fibers, which are composed of a series of contractile units called sarcomeres, can only contract (actively). It is thanks to the different arrangements in which fibers are organized (muscular architectures), and to their cooperation in muscular groups of different shapes and sizes, that muscle systems and animals exhibit such a plethora of active movements [1–5].

The contraction performance of muscles differs based on the number of fibers and their configuration within the muscle structure. The maximum contraction achievable is mainly defined by the arrangement of the fibers with respect to the direction of the tendons that transmit the action. If the muscular fibers and the tendons are parallel, then the contraction obtainable is maximum as occurs for the fusiform muscle (i.e., biceps). The configuration of the fibers also affects how they can be packed, varying their density within the muscle. A muscle whose fibers are shorter and tilted with respect to tendons can contain more fibers than a muscle with a parallel arrangement. In the former case, the contraction displacement is smaller due to the fibers' slant, yet the produced forces are higher. The number of fibers, indeed,

determines the maximum force generated. A pennate muscle, whose fibers are arranged at a certain angle, named pennation angle, accommodate more, shorter fibers and usually exerts higher forces than a fusiform muscle [6–13].

The primary regulation method of natural muscles involves fiber recruitment, consisting of fully activating only a certain number of fibers. This behavior is the key to the efficient regulation of the force generated by the muscle. It directly modulates the outcome force, whereas the contraction indirectly results from the forces' balance. While performing a task, the number of active fibers depends on the actions carried out, increasing or decreasing if higher or lower forces are required. Therefore, the natural contraction regulation relies on the muscle fiber recruitment, not on the modulation of the input of the single fiber. In the development of biomimetic muscle systems, considering the large number of muscles that usually constitute animals' bodies, each one containing from a few up to thousands of fibers, this regulation strategy could be imitated for effective force modulation with reduced control complexity [14–20].

Being able to replicate muscular architectures in artificial machines, making them able to move with the same grace and naturalness as animals, represents an open engineering challenge. Over the years, multiple artificial muscles have been developed aiming to mimic the muscle behavior [21–24]. They are widely spread in bioinspired and soft robotics as actuators capable of performing contractions similar to muscular ones.
Among them, the most adopted are the artificial pneumatic muscles (PAMs), mainly because they can generate high forces and good contractions while being lightweight and not excessively expensive. The first and most notorious PAM is the McKibben PAM, developed in 1950s. Since then, despite the many design variations that have been proposed, it remains the most employed [25–31].

Recently, multifilament PAMs have been proposed, where the artificial fibers consist of McKibben PAMs miniaturized in diameter and arranged in bundles of parallel units constrained at the ends to mimic the structure of fusiform skeletal muscles [32]. These bundles of fibers have been adopted to artificially reproduce some human movements by attaching them to skeletal supports. In this way, the single actuator is no longer intended as a single muscle but as a replica of the muscle fiber, opening possibilities of realizing biomimetic muscle architectures to build up multi-functional muscular systems. This could also allow the implementation of regulation strategies more similar to those of natural muscles based on the number of active fibers. In pneumatic systems, indeed, the regulation is carried on by modulating the input analogically using pressure regulators, which complicate the control and are much more expensive than simple on/off valves. This control method tends to be effective when systems have few degrees of freedom but becomes more and more complex and expensive as their number grows [33–36].

Despite these recent results, building up biomimetic systems composed of several pneumatic actuators still requires a rather laborious manufacturing process whose effort exponentially increases accordingly with the number of actuators employed in the system. Their manufacturing, indeed, often requires purposely designed machines for the mass production of the individual actuators as well as several manual steps both to complete the fabrication of each fiber and to assemble them mimicking the muscle architectures. Furthermore, the troublesome fabrication and the limited versatility of the layout of many state-of-the-art actuators intrinsically hinder their implementation in muscle architecture that require arrangements more articulated than the parallel disposition [37–43].

Recently, the GRACE PAMs have been proposed to match some of the versatility of the natural muscles. They have a scalable and tunable design, and they can be 3D printed with different materials and in complex configuration [44]. Here we adopt GRACE pneumatic actuators as individual contractile units (CUs) to realize hierarchical PAMs that mimic natural muscle architectures. In these artificial muscles, the CUs, akin to the sarcomers, are placed in series to form artificial fibers, which, in turn, are biomimetically arranged to mimic diverse architectures of natural muscles. We show that entire artificial muscular architecture can be 3D printed at once and without additional assembly. In particular, we demonstrate three different artificial architectures: the fusiform, the parallel, and the bipennate. We characterize them through isotonic and isometric tests and compare their performances to highlight their peculiarities. These architectures allow us to also implement and test biomimetic regulation methods. Here we adopt both the commonly used modulation of the pressure input and a more biomimetic method based on the selective activation (recruitment) of the fibers, discussing advantages and limitations of the two methods. Therefore, this work demonstrates the development of biomimetic PAMs, from the CUs' design all the way up to 3D-printed hierarchical architectures and to recruitment-based regulation.

2) Design and Fabrication (Methods)

1.1 Contractile Unit Design

For the design of the three muscle architectures, we have chosen the GRACE design optimized to maximize contraction, named GRACE-C, to represent the basic CU (Fig.1). The design, presented in [44], is openly accessible at

https://doi.org/10.5281/zenodo.6693428. Firstly, we have generated the geometry of the desired GRACE using the model specifically developed for this class of PAMs in [44]. The model, indeed, relates the GRACEs deformations, achieved by pressurization and depressurization, to their geometry, allowing the actuators customization based on the contraction/extension needs. In the model, we have set the rest length of the actuator to 20 mm, half the size of the original GRACEs. Considering the confined printing workspace, an even smaller size of the CUs could have allowed stacking more of them but would have also made the muscle architectures more challenging to fabricate by low-cost desktop 3D printers.

Knowing the geometric parameters of the desired actuator resulting from the GRACE model and reported in Table 1, we have drawn the preliminary design using Computer Aided Design (CAD) software. We have then refined the design by defining a reasonable value for the average membrane thickness through Finite Element Analysis (FEA). A membrane thickness of 0.7 mm was chosen, a value that permits achieving significant forces while requiring only low-pressure inputs. Thicker membranes would lead to higher forces but require higher pressure inputs, whereas thinner membranes would reach lower forces and could be more difficult to print using a desktop 3D printer, particularly when many actuators are embedded in a complex structure.

To fabricate both the single actuator and the three different muscle prototypes, we employed a stereolithography-based

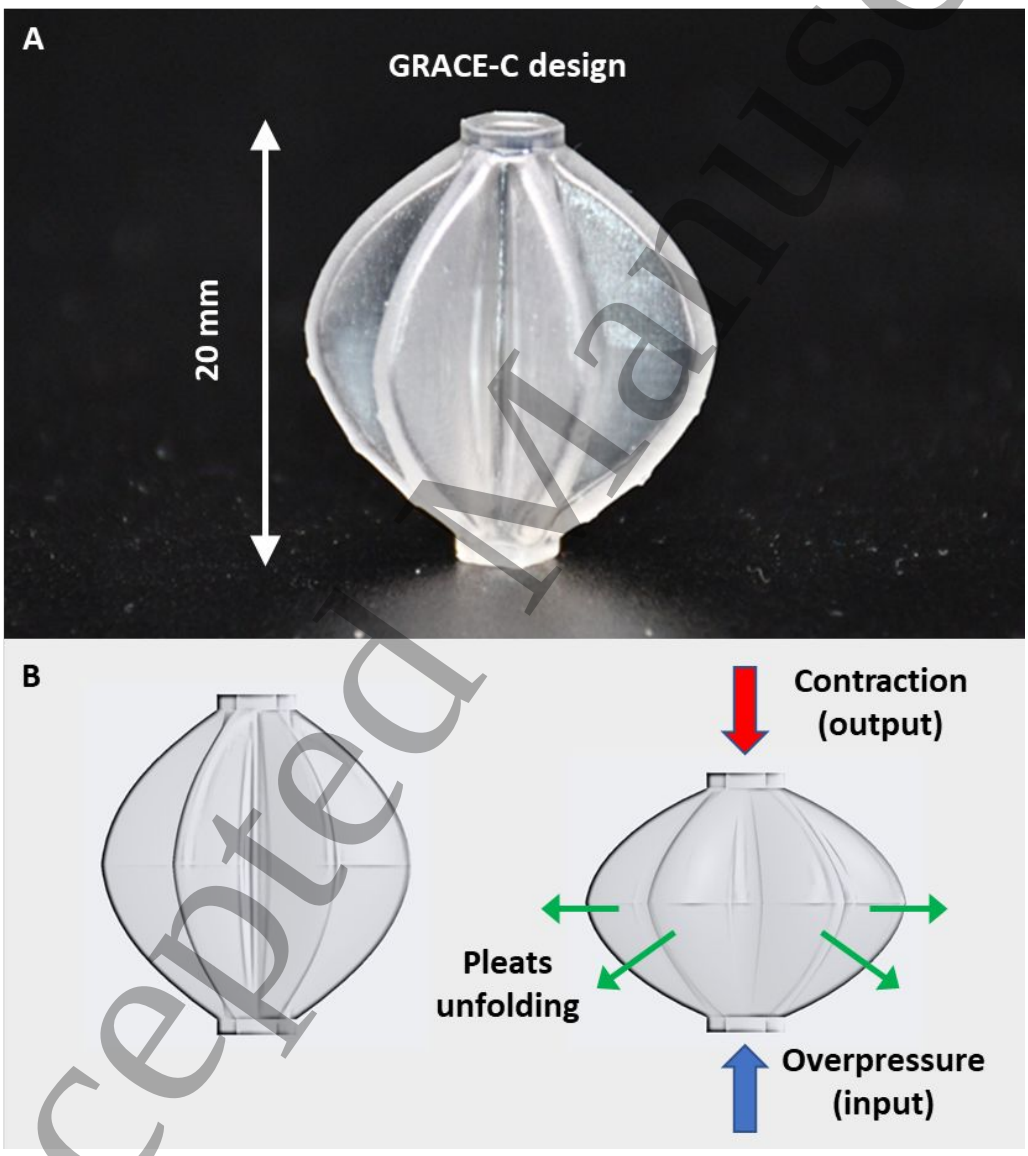

Fig. 1. Contractile Unit (CU). (A) 2 cm-long CU based on the GRACE-C design (GRACE with maximize contraction), 3D-printed with a SLA printer and a flexible material (Formlabs Form 3 and Flexible 80A resin); in the right corner is reported its cross-section. (B) Schematic illustration of the actuation mechanism of the CU.

desktop 3D printer (Formlabs Form 3) and a commercial flexible resin (Formlabs Flexible 80A

N° Pleats	**6**
Average thickness	**0.7 mm**
Length (L)	**20 mm**
a_1	$0.9 * {}^{L}/_{2} = 9\ mm$
a_2	$0.19 * {}^{L}/_{2} = 1.9\ mm$
b_1	$0.242 * {}^{L}/_{2} = 2.42\ mm$
b_2	$0.24 * {}^{L}/_{2} = 2.4\ mm$
R_1	$0.899 * {}^{L}/_{2} = 8.99\ mm$
R_2	$0.9 * {}^{L}/_{2} = 9\ mm$

2.1 Muscle Architectures Designs

In designing the three muscle architectures, we adopted a composition of CUs based on three elementary layouts: parallel, series, and pennate (Fig.2). In the parallel layout, the total force is the sum of the forces exerted by each unit whereas the total contraction is the same as that of a single unit. In the series layout, the total contraction achieved is the sum of those of the units whereas the total force is the same as that of a single unit. In the pennate one, the units are tilted with the respect of the tendon, thus both total force and contraction are attenuated by the cosine of the angle between the unit and the tendon, named pennation angle. For the design of the muscle architectures, we have set the same length and involved the same number of CUs, decided a priori. This is to allow for a fair performance comparison and to show examples of possible arranging strategies given some dimension constraints such as maximum available length. The length of the structures involved in the contraction was set at 158 mm considering the maximum workspace of the printer which is 145 x 145 x 185 mm. The length of the three structures has then been increased during the design process by adding end-shapes needed only to interlock the prototypes to the testing machine without influencing the contraction and thus the performance comparison. For each design, we have employed 36 GRACE-C units, a quantity sufficiently large to efficiently show the different architectures behavior and easily arrangeable in the three different configurations given the chosen size of the actuator and the total length of the structure.

2.2 Fusiform Muscle Design

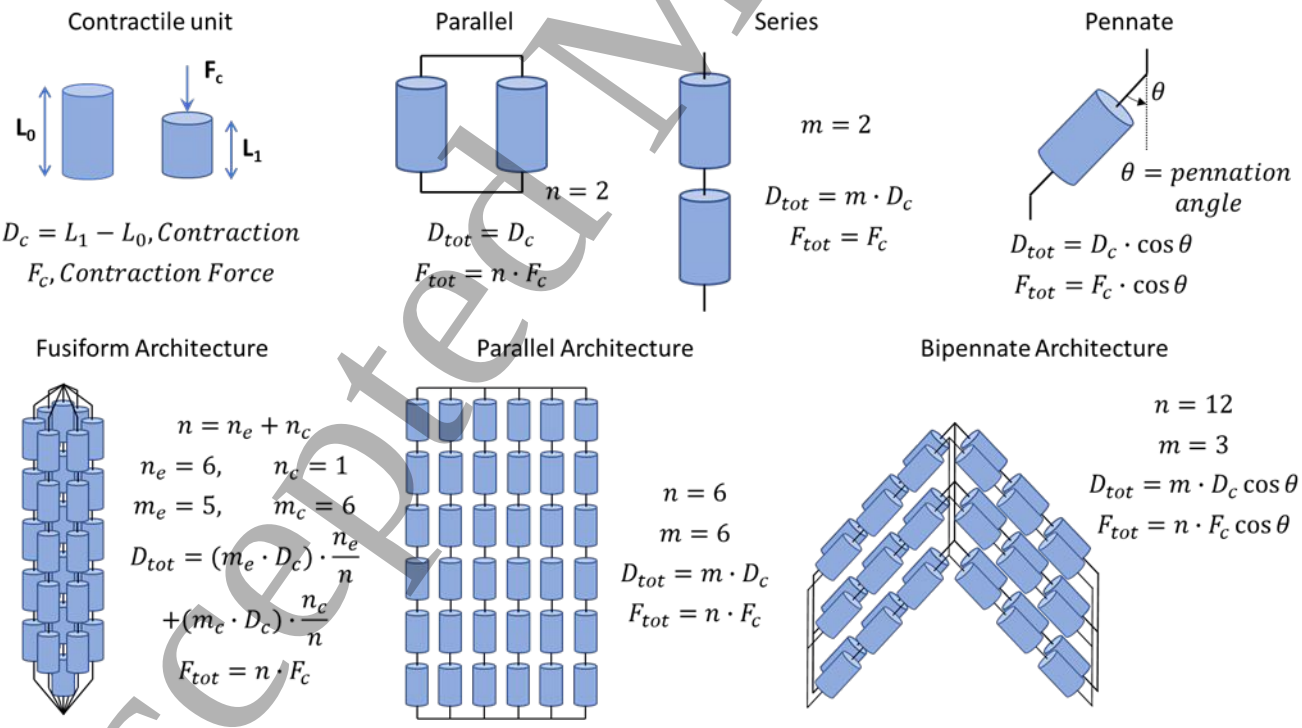

Fig. 2. Muscle architectures schemes. Schemes of the basic arrangements and of the three muscle architectures for the CUs and the formulas of the contractions and forces achieved.

Tab. 1. CU design parameters. Main design parameters of the GRACE-C adopted as CU, resulting from the GRACE model presented in [44].

The fusiform architecture is composed of a total of seven fibers, six arranged in a hexagon shape with an additional one placed in the center (Fig.3, left). Each fiber consists of five units in series except for the central one, which contains six of them. This distribution strategy allowed the spatial phase shift along the muscle axis of the actuators composing the external fibers with respect to those of the central one, resulting in increased compactness of the overall structure. The fibers are parallelly disposed and the external ones have connectors that converge towards the central fiber at the two extremities joining the structure and forming an overall tapered shape. The fibers are not radially linked together in the central part of the structure and the connectors at the ends let them freely deform even if actuated alone. The overall length of the structure is 158 mm plus two blocks of 8 mm height at both ends which are not involved in the contraction and are only needed to allow the clamping into the mechanical testing machine used for the characterization. The holes for the plug-in of the pneumatic lines were positioned at the bottom of each fiber.

2.3 Parallel Muscle Design

The parallel configuration consists of six fibers parallelly arranged in a single flat layer (Fig.3, center). Each fiber is composed of six units in series rotated by 30° (along their axis) with respect to those of the adjacent fiber to increase the compactness of the structure. In this way, the pleats' crests of the actuators of one fiber are aligned with the pleats' valleys of the actuators of the adjacent fibers, allowing stacking the fibers closer.

Unlike the two other designs, here we have added planar connectors between the fibers at the junction of subsequent CUs. The connectors help to reduce the compression buckling of the fibers not actuated during the contraction regulation driven by activating only some fibers. This phenomenon, which intensifies as the fibers' length increases, arises from the compression instability of the unactuated fibers that, forced to passively contract by the actuated ones, tend to bend. The buckling effect does not occur when the fibers are all actuated with the same pressure input, thus when controlled through the traditional method by using a single pressure regulator. As far as we have experienced for the three muscle architectures developed, this behavior only leads to an increased encumbrance during the contraction without particular loss of performance or integrity of the prototypes. We have decided to add connectors in the parallel design since it involves longer fibers than the others, thus more sensitive to the buckling effect. The connectors can be possibly implemented in the two other designs to minimize the bulkiness during actuation if needed.

The overall length is 158 mm, plus two adapters of 4 mm at the two extremities that do not participate to the contraction and allow the structure to be clamped into the mechanical testing machine. The holes for the pneumatic connection are located at one of the two bases of the structure.

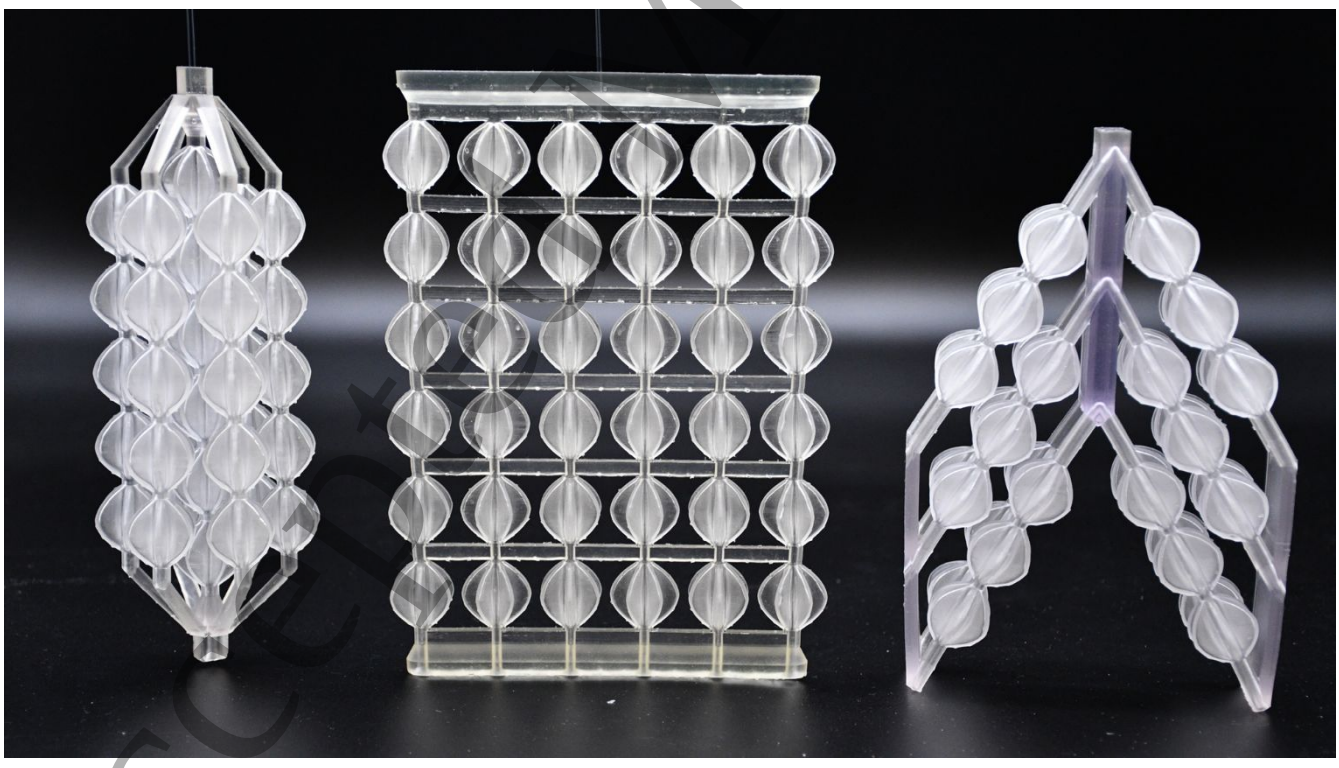

Fig. 3. Artificial muscle architectures. The three artificial muscle architectures each composed of 36 CUs, printed through SLA with Form 3 printer and Flexible 80A resin (Formlabs).

2.4 Bipennate Muscle Design

The bipennate architecture is constituted by twelve fibers, each one made up of three units in series (Fig.3, right). The fibers are arranged in two parallel layers each one containing two sets of three fibers symmetrical with respect to the central tendon, for a total of six fibers per layer. The fibers are accommodated between a central flat tendon and two external ones parallel to each other. The tendons are the only elements connecting the fibers together. They convert the individual fiber contractions into the total deformation of the structure.

Each fiber is oriented at an angle of 30 ° with respect to the central tendon and therefore to the direction of the transmission of the contraction. This is a typical reference value for the angle between fibers and tendons, called pennation angle in the natural pennate architecture. Incrementing the pennation angle in the design reduces the contraction transmitted by the fibers to the tendon but also allows for parallelly stacking more of them, increasing their density and therefore producing greater forces.

The central tendon has internal hollow channels that connect the pneumatic lines of the fiber pairs of the two layers that are at the same height, symmetrical with respect to the central tendon. This is both to facilitate the post-printing cleaning process of the hollow channel inside each fiber and to ensure that these fibers share the same pressure input.

In this way, the fibers are grouped in three pneumatically independent groups, each consisting of the four fibers which are connected to the tendons at the same height. The four fibers of a group do not need to be actuated with different pneumatic inputs as this would only lead to bending of the structure. The overall length is 158 mm, plus an 8 mm extension of the central tendon that is not involved in the contraction and allow the structure to be clamped into the mechanical testing machine from one side. To clamp the two external tendons to the tensile machine we have realized an additional interlocking mechanism with Polylactic Acid (PLA) through fused deposition modeling techniques (FDM). The holes to plug in the pneumatic lines are located along the lateral tendons.

3) Characterization

To characterize and compare the performance of the three muscle architectures we carried out isotonic and isometric tests. In the isotonic tests, the specimens are actively contracted while the tensile machine maintains a constant force applied and records the displacement achieved. In the isometric tests, the testing machine keeps the length of the specimens constant while they are actively contracted and records the force exerted.

Here, we have carried out the isotonic test with no load applied to measure the free contraction reached, and the isometric tests with zero displacements permitted to measure the blocking force generated. As a first step, we performed these two tests on the single CU to characterize the units' actuation performance. We then repeated the two tests multiple times for each of the three muscle architectures, activating different numbers of fibers. In this way, we were able to infer the contraction performance obtained both by the modulation of the pressure input and by the fiber recruitment. In each test, the prototypes were pressurized for five actuation cycles, interspersed with pauses to permit the structure to relax back to the starting configuration. The time windows of the cycles and pauses were set considering the stress relaxation and creep time constants of the viscoelastic Flexible 80A material. Actuation cycles and pauses last respectively 90 s and 180 s in the isometric tests whereas they last 180 s and 300 s in the isotonic tests.

3.1 Single CU Tests

During the isotonic test (Fig.4, A and B), the CU performed a maximum contraction of 5.2 mm, equal to 26% of its length, with a pressure input of 26.8 kPa. It reached a maximum pulling force of 6.8 N with a pressure input of 26.7 kPa during the isometric test (Fig.4, C and D).

3.2 Fusiform Prototype Tests

For the fusiform architecture, we carried out the isotonic and isometric tests actuating the prototype with four different combinations of fibers, for a total of eight tests. In choosing the fibers to be pressurized together, we preferred symmetrical combinations that induced only simple contraction without any additional bending. The groups of active fibers during the tests were: the central one alone, the central one plus three fibers at 120° degrees for a total of 4 fibers, the central one plus the four fibers forming a rectangle around it for a total of five, and lastly all the seven fibers together.

In the isotonic tests (Fig.5 and fig.11A), the fusiform prototype reached maximum contractions of 25 mm, 25.5 mm, 26.8 mm, and 28.6 mm, respectively equal to 15.8%, 16.1%, 17%, and 18.1% of its length, with an increasing number of active fibers and at pressures of about 26 kPa.

In the isometric tests (Fig.6 and fig.11B), the fusiform prototype exerted maximum forces of 6.6 N, 14.2 N, 17.4 N, and 24.8 N, with an increasing number of active fibers and at pressures of around 26 kPa.

3.3 Bipennate Prototype Tests

For the characterization of the bipennate arrangement, we carried out the tests actuating the prototype with three different combinations of fibers for a total of six tests. Similar to the fusiform case, the symmetrical combinations of active fibers have been chosen to avoid inducing bending in the structure. We chose to pressurize first the group composed of the four fibers that connect the bases of the external and

central tendons, then also the group of the four fibers in the intermediate position with respect to the tendons for a total of eight and at the end even the last group for a total of twelve fibers together.

In the isotonic tests (Fig.7 and fig.11C), the bipennate prototype achieved maximum contractions of 15.8 mm, 18.2 mm, and 19.2 mm, respectively equal to 10%, 11.5%, and 12.2% of its length, with an increasing number of active fibers and at pressures of around 24 kPa. In the isometric tests (Fig.8 and fig.11D), the bipennate prototype exerted maximum forces of 14.6 N, 29.6 N, and 43.6 N with an increasing number of active fibers and at pressures of around 26 kPa.

3.4 Parallel Prototype Tests

For the characterization of the parallel architecture, the prototype was actuated with three different combinations of fibers for a total of six tests. Similar to the other cases, the combinations of fibers to be actuated were chosen to avoid unwanted bending. The prototype was initially actuated with two fibers, the second and the fourth, then with four fibers, the two centrals plus the two external ones, and finally with all six fibers together. In the isotonic tests (Fig.9 and fig.11E), the parallel prototype performed maximum contractions of 21.5 mm, 30.3 mm, and 30.2 mm, respectively equal to 13.6%, 19.2%, and 19.1% of its length, with an increasing number of active fibers and at pressures of around 28 kPa. In the isometric tests (Fig.10 and fig.11F), the parallel prototype exerted maximum forces of 13.3 N, 25.8 N, and 38.8 with an increasing number of active fibers and at pressures of around 28 kPa.

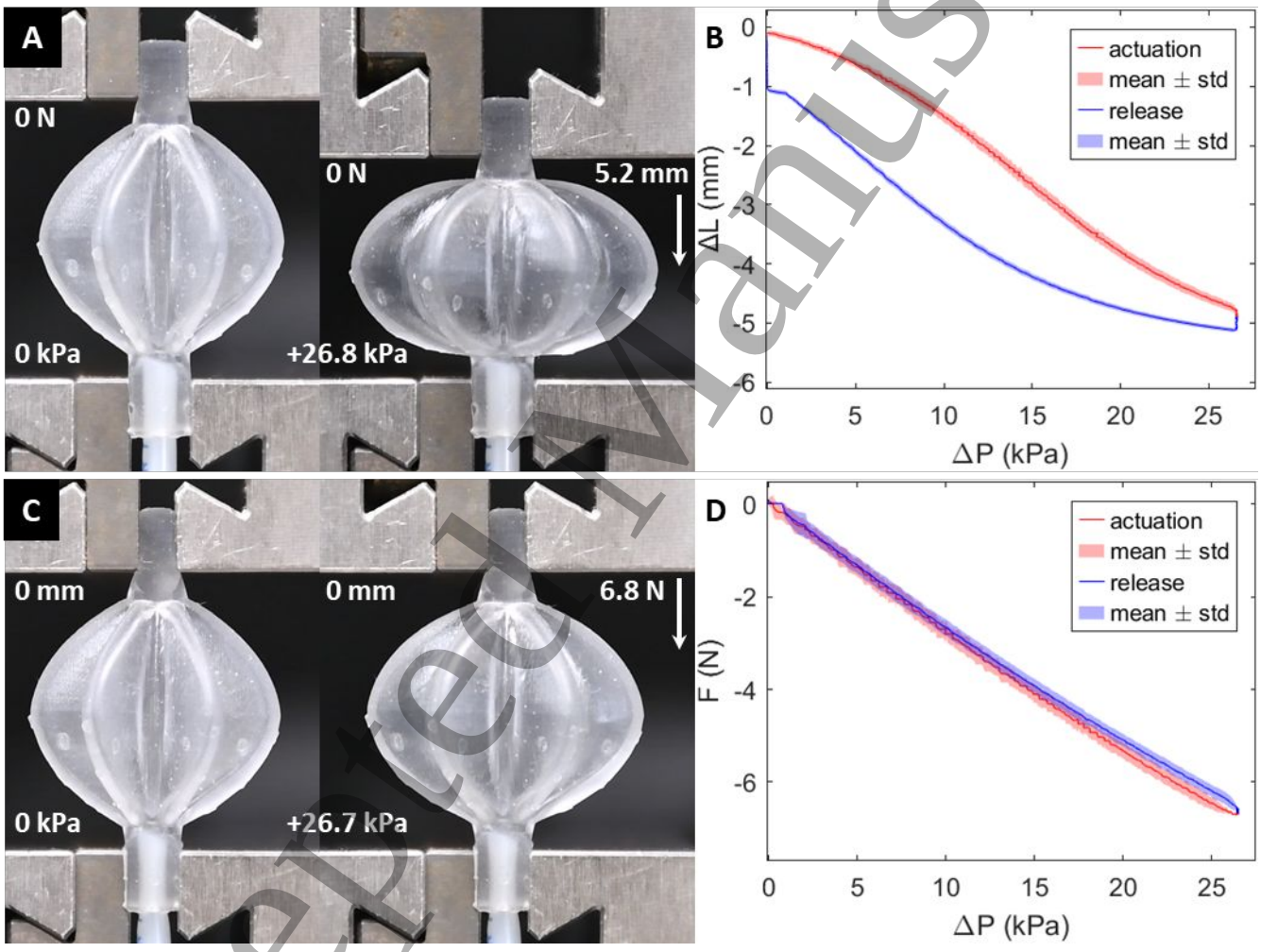

Fig. 4. CU characterization. Isotonic test for the single CU with no load applied: (A) at rest (left) and pressurized (right); (B) actuation and release curves (mean over 5 cycles). Isometric test for the single CU with no stretch applied: (C) at rest (left) and pressurized (right); (D) actuation and release curves (mean over 5 cycles).

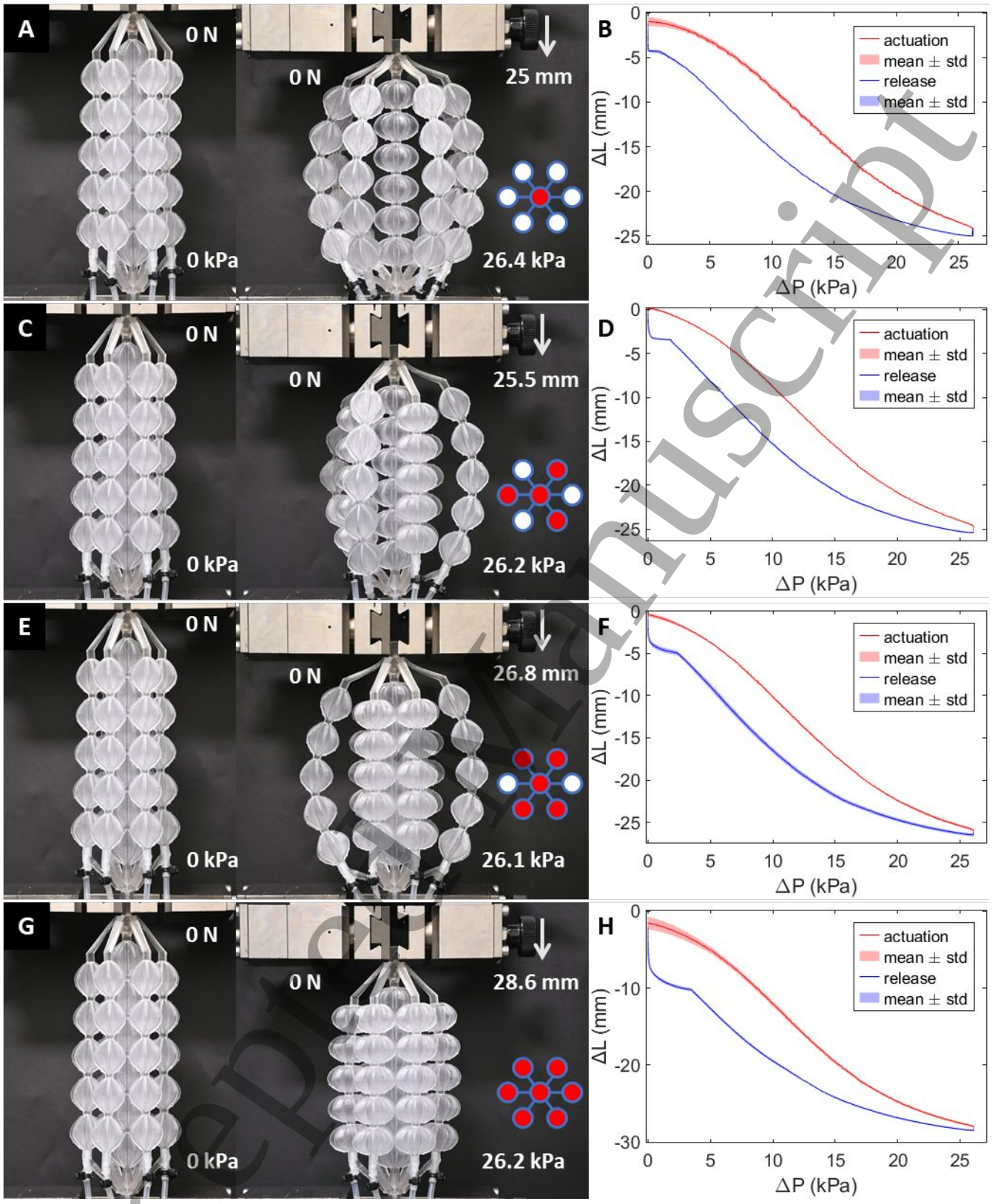

Fig. 5. Fusiform architecture isotonic characterization. No-load isotonic test for the fusiform prototype with only the central fiber actuated: (A) at rest (left) and pressurized (right); (B) actuation and release curves (mean over 5 cycles). No-load isotonic test for the fusiform prototype with four fibers actuated: (C) at rest (left) and pressurized (right); (D) actuation and release curves (mean over 5 cycles). No-load isotonic test for the fusiform prototype with five fibers actuated: (E) at rest (left) and pressurized (right); (F) actuation and release curves (mean over 5 cycles). No-load isotonic test for the fusiform prototype with all seven fibers actuated: (G) at rest (left) and pressurized (right); (H) actuation and release curves (mean over 5 cycles). The fibers actuated are reported as red dots in the schemes at the right of (A), (C), (E), and (G), whereas the unactuated ones are shown as white dots.

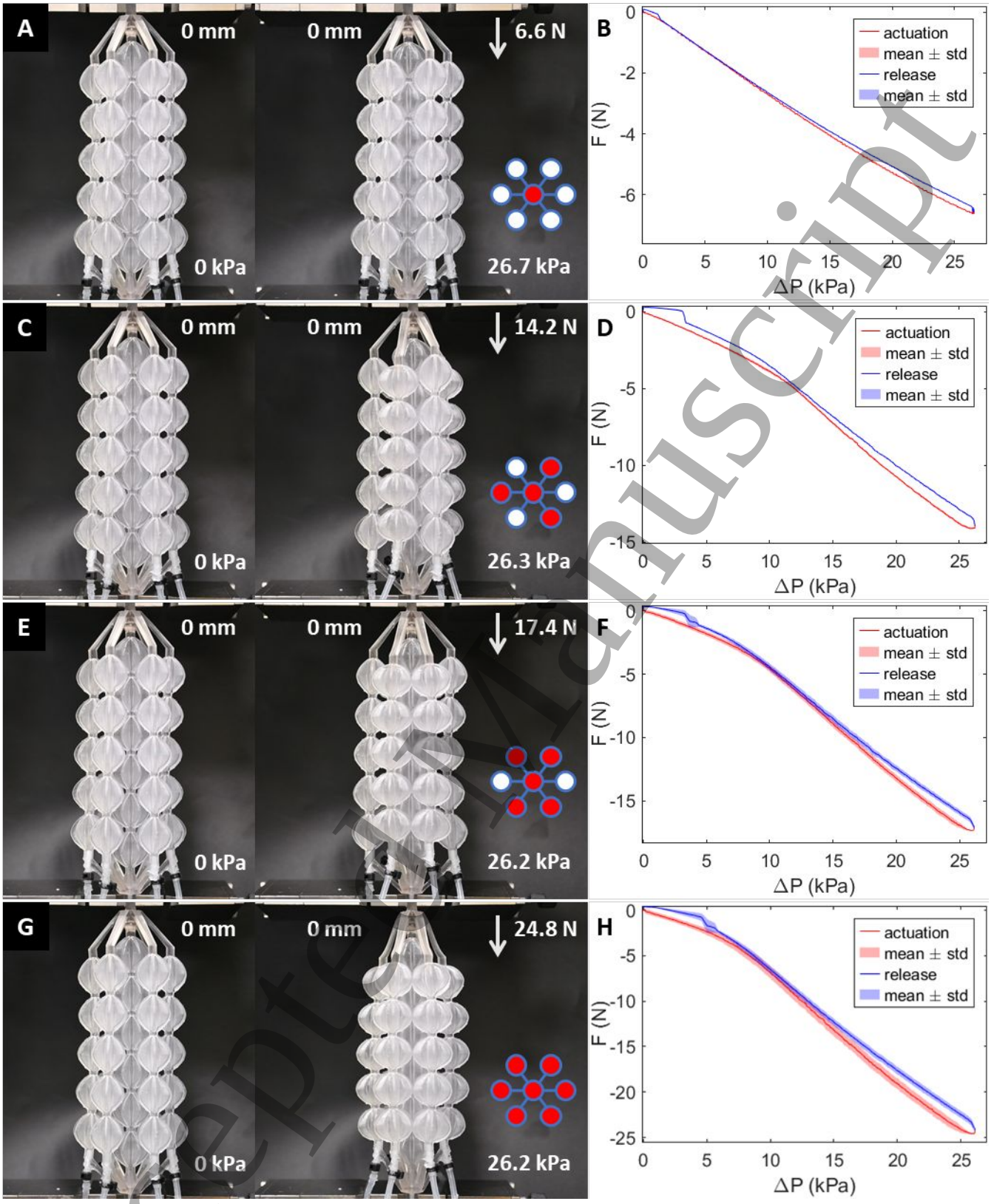

Fig. 6. Fusiform architecture isometric characterization. No-stretch isometric test for the fusiform prototype with only the central fiber actuated: (A) at rest (left) and pressurized (right); (B) actuation and release curves (mean over 5 cycles). No-stretch isometric test for the fusiform prototype with four fibers actuated: (C) at rest (left) and pressurized (right); (D) actuation and release curves (mean over 5 cycles). No-stretch isometric test for the fusiform prototype with five fibers actuated: (E) at rest (left) and pressurized (right); (F) actuation and release curves (mean over 5 cycles). No-stretch isometric test for the fusiform prototype with all seven fibers actuated: (G) at rest (left) and pressurized (right); (H) actuation and release curves (mean over 5 cycles). The fibers actuated are reported as red dots in the schemes at the right of (A), (C), (E), and (G), whereas the unactuated ones are shown as white dots.

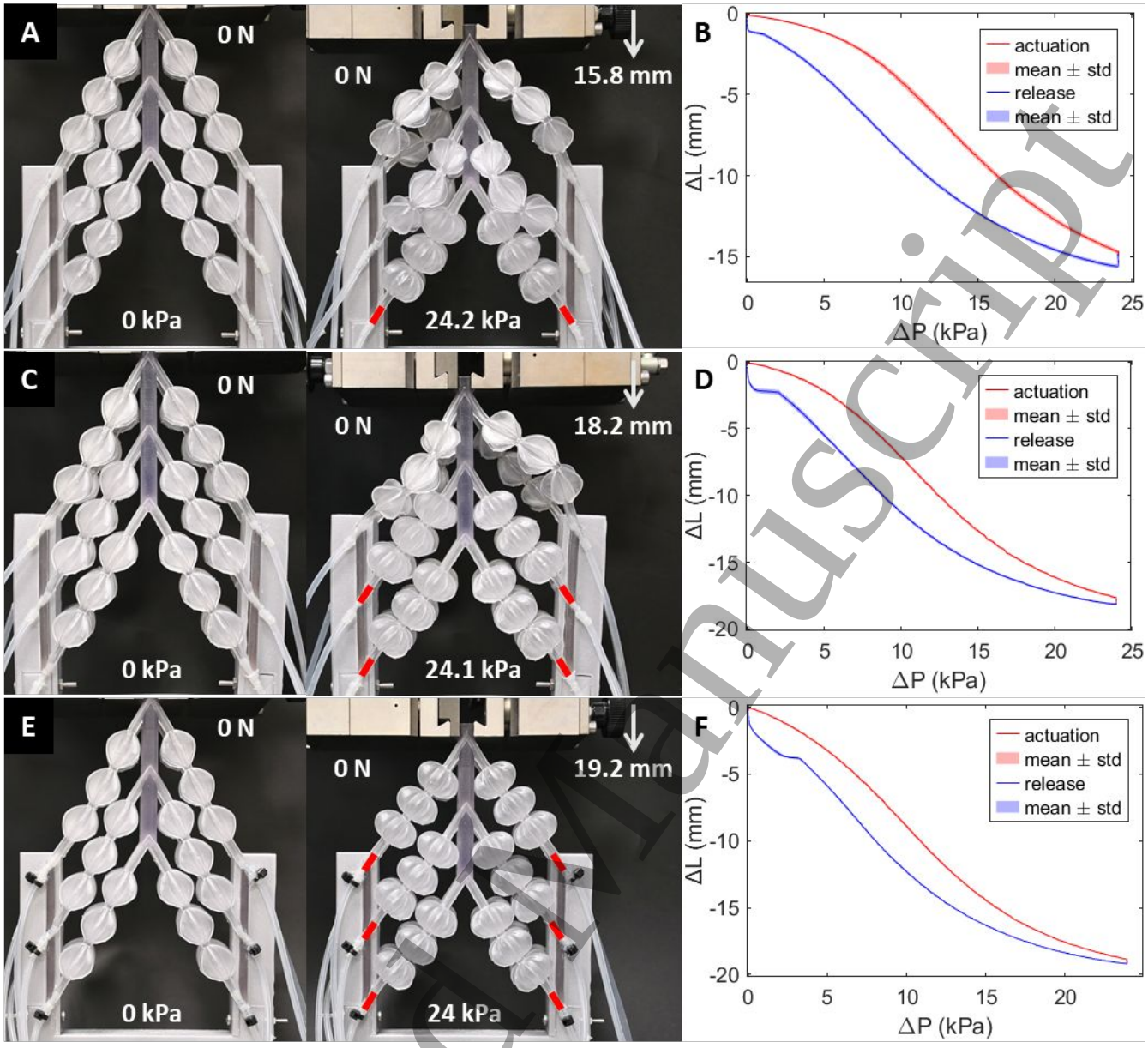

Fig. 7. Bipennate architecture isotonic characterization. No-load isotonic test for the bipennate prototype with four fibers actuated (red marks): (A) at rest (left) and pressurized (right); (B) actuation and release curves (mean over 5 cycles). No-load isotonic test for the bipennate prototype with eight fibers actuated (red marks): (C) at rest (left) and pressurized (right); (D) actuation and release curves (mean over 5 cycles). No-load isotonic test for the bipennate prototype with all twelve fibers actuated (red marks): (E) at rest (left) and pressurized (right); (F) actuation and release curves (mean over 5 cycles).

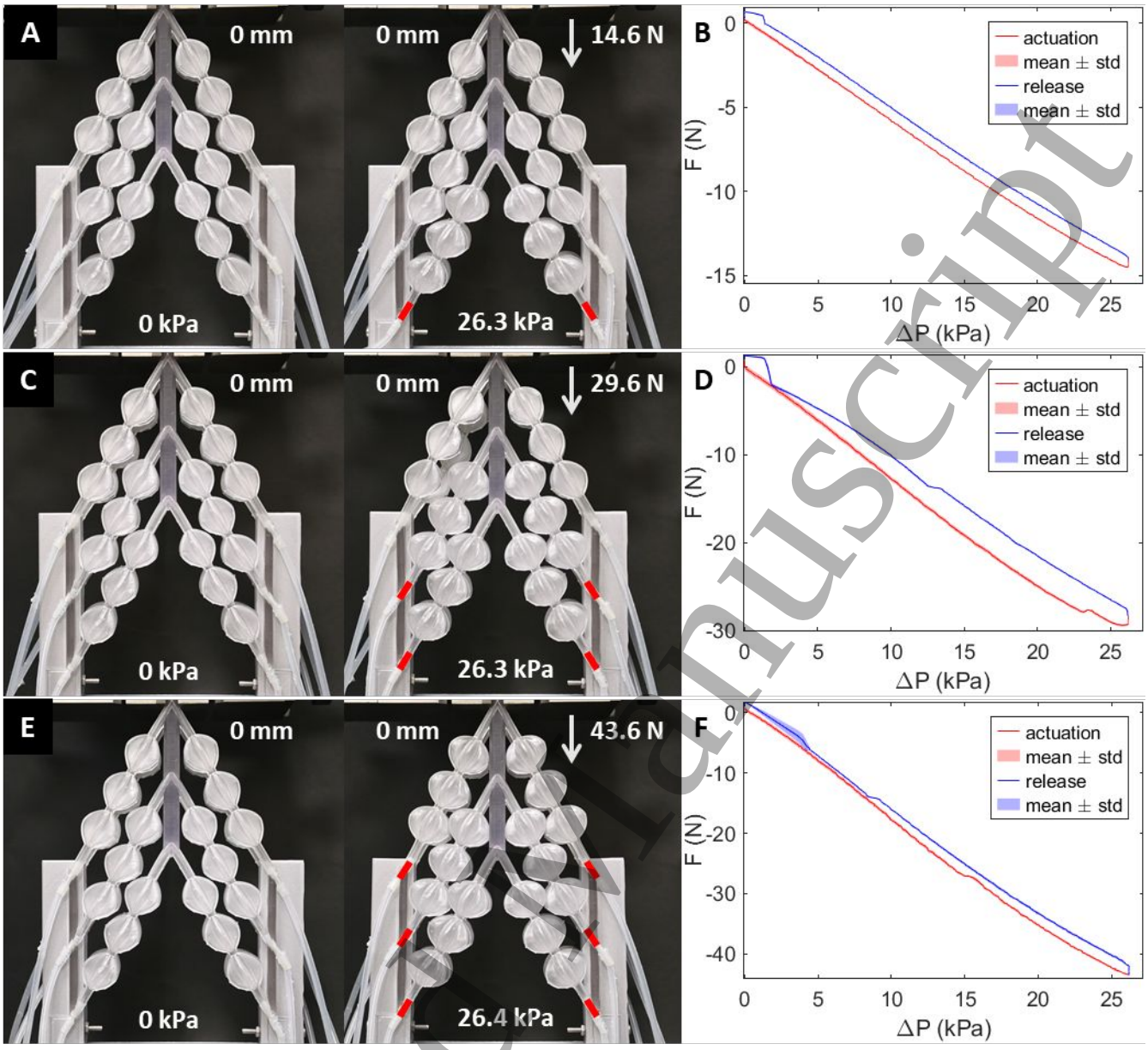

Fig. 8. Bipennate architecture isometric characterization. No-stretch isometric test for the bipennate prototype with four fibers actuated (red marks): (A) at rest (left) and pressurized (right); (B) actuation and release curves (mean over 5 cycles). No-stretch isometric test for the bipennate prototype with eight fibers actuated (red marks): (C) at rest (left) and pressurized (right); (D) actuation and release curves (mean over 5 cycles). No-stretch isometric test for the bipennate prototype with all twelve fibers actuated (red marks): (E) at rest (left) and pressurized (right); (F) actuation and release curves (mean over 5 cycles).

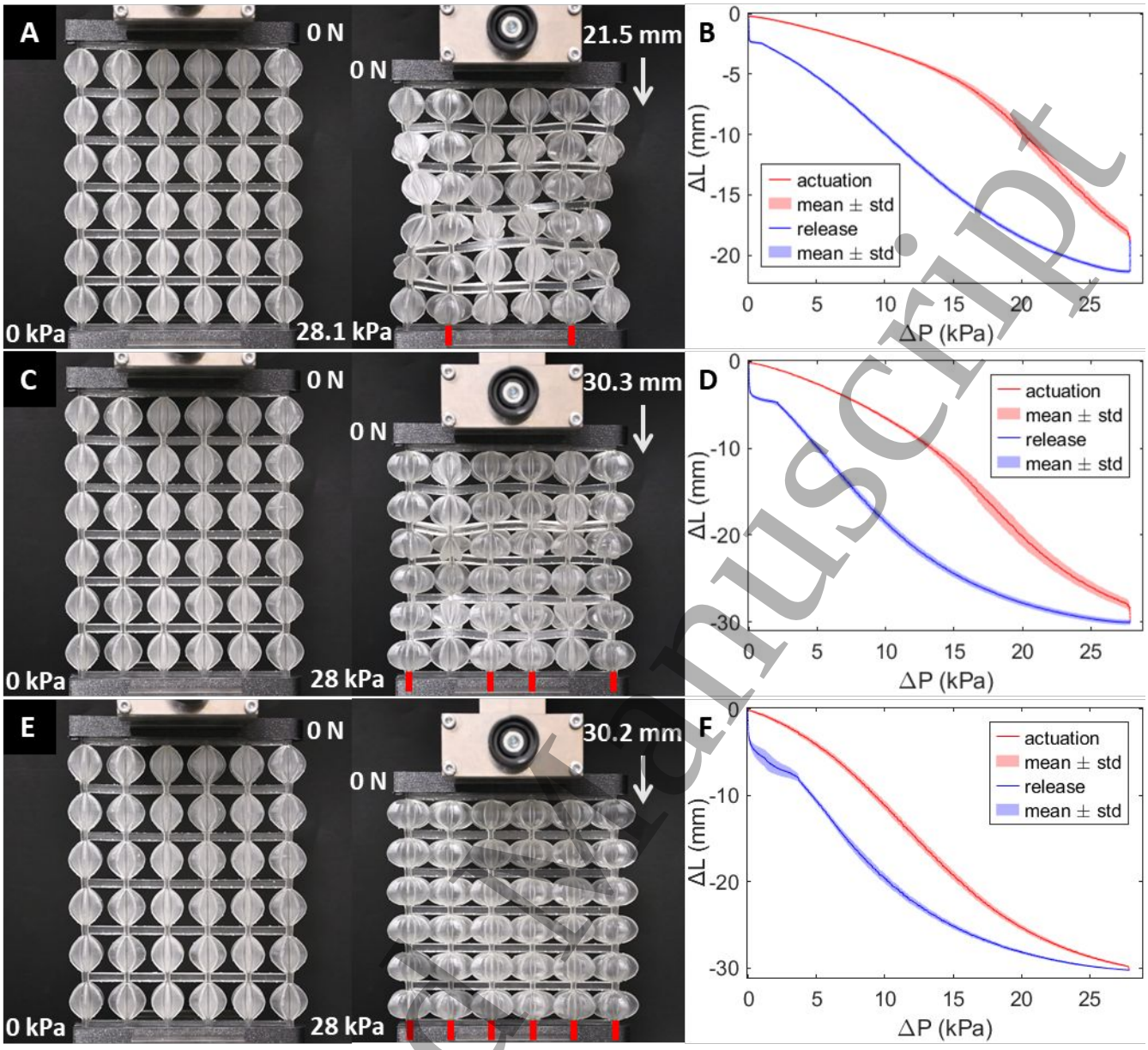

Fig. 9. Parallel architecture isotonic characterization. No-load isotonic test for the parallel prototype with two fibers actuated (red marks): (A) at rest (left) and pressurized (right); (B) actuation and release curves (mean over 5 cycles). No-load isotonic test for the bipennate prototype with four fibers actuated (red marks): (C) at rest (left) and pressurized (right); (D) actuation and release curves (mean over 5 cycles). No-load isotonic test for the bipennate prototype with all six fibers actuated (red marks): (E) at rest (left) and pressurized (right); (F) actuation and release curves (mean over 5 cycles).

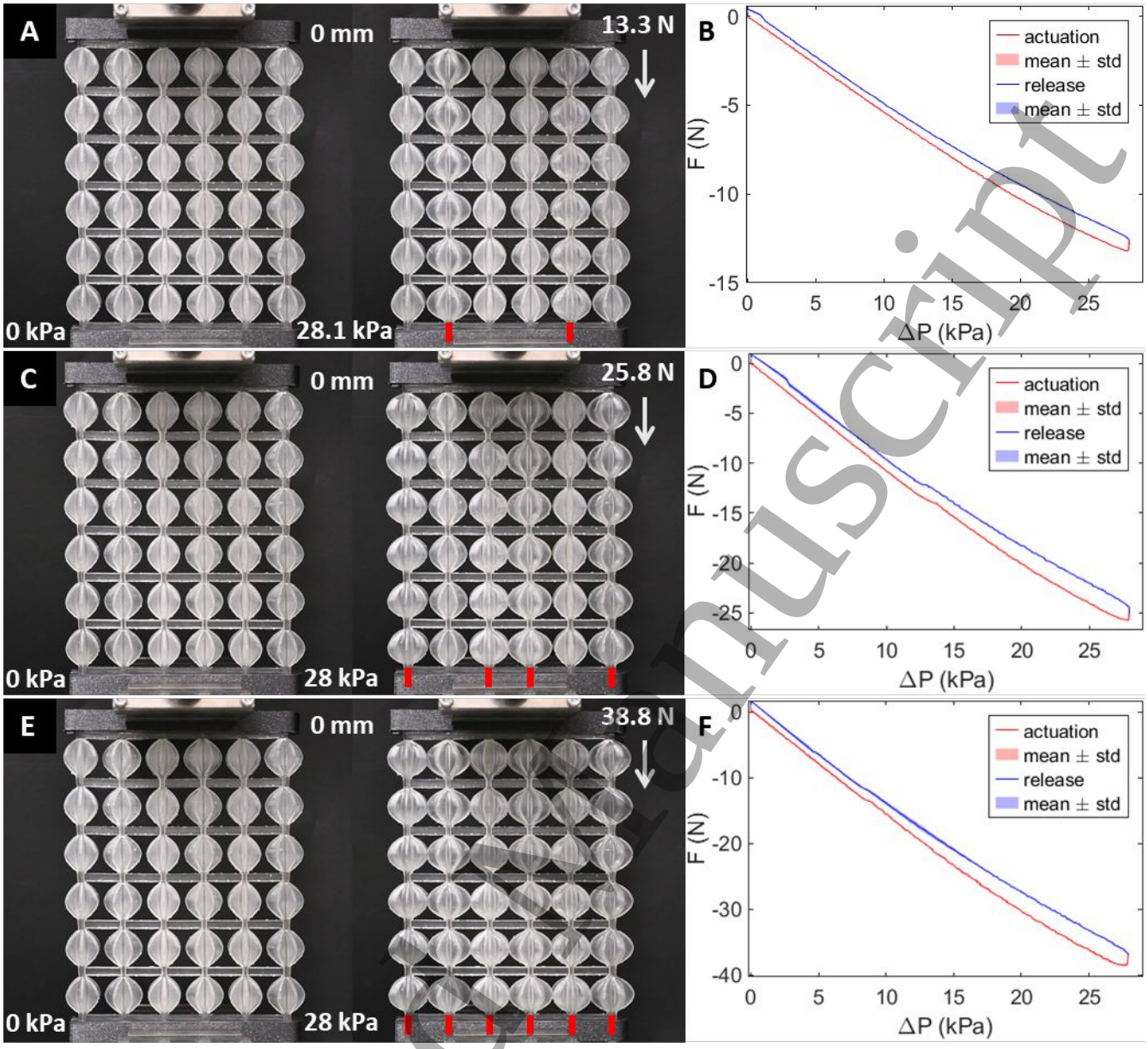

Fig. 10. Parallel architecture isometric characterization. No-stretch isometric test for the parallel prototype with two fibers actuated (red marks): (A) at rest (left) and pressurized (right); (B) actuation and release curves (mean over 5 cycles). No-stretch isometric test for the bipennate prototype with four fibers actuated (red marks): (C) at rest (left) and pressurized (right); (D) actuation and release curves (mean over 5 cycles). No-stretch isometric test for the bipennate prototype with all six fibers actuated (red marks): (E) at rest (left) and pressurized (right); (F) actuation and release curves (mean over 5 cycles).

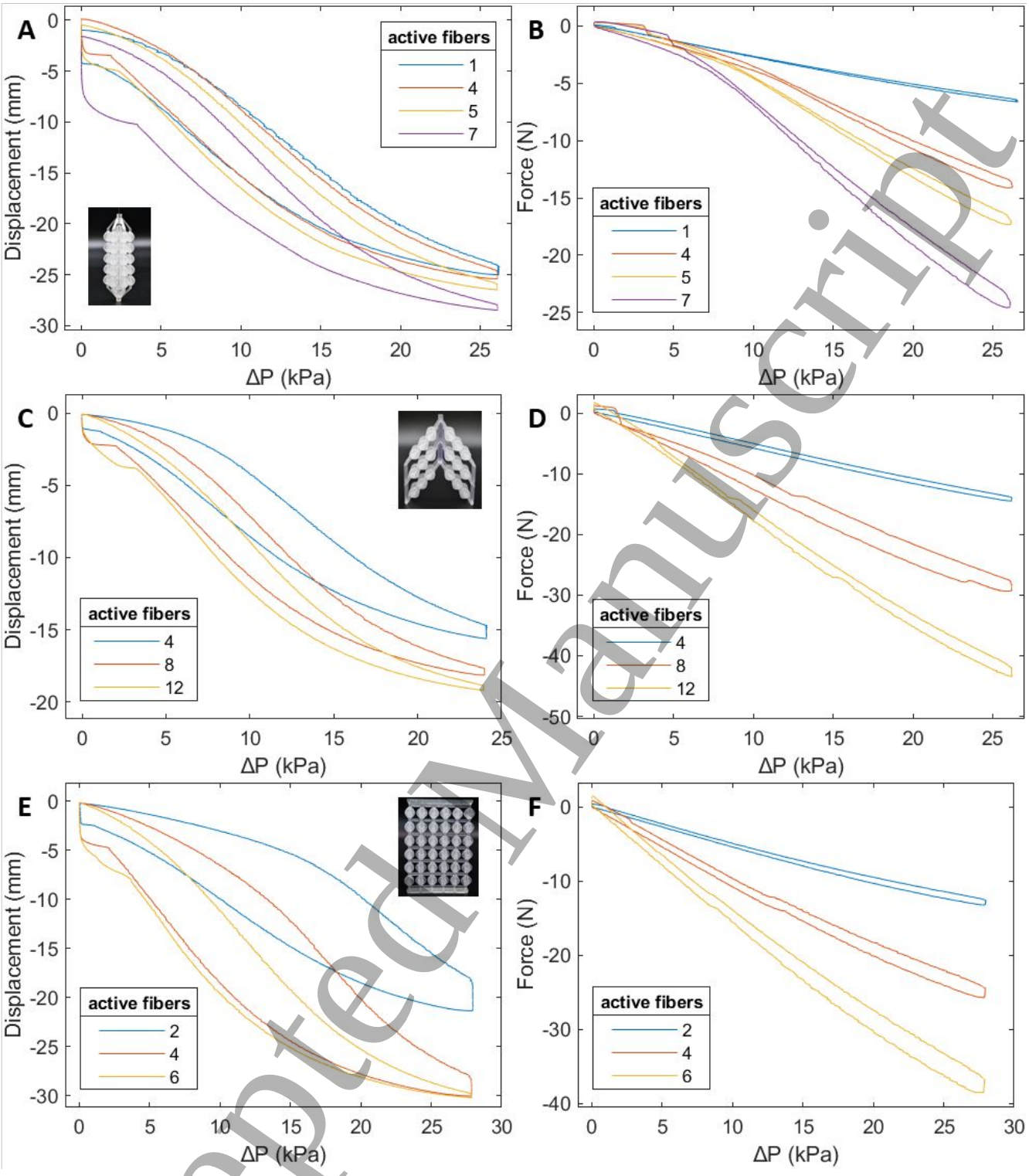

Fig. 11. Regulation by fiber recruitment. Actuation cycles for the fusiform prototype actuated with different number of fibers: (A) contraction displacement resulted from isotonic tests, (B) contraction force resulted from isometric tests. Actuation cycles for the bipennate prototype actuated with different number of fibers: (C) contraction displacement resulted from isotonic tests, (D) contraction force resulted from isometric tests. Actuation cycles for the parallel prototype actuated with different number of fibers: (E) contraction displacement resulted from isotonic tests, (F) contraction force resulted from isometric tests.

4) Discussion

The isotonic and isometric tests on the 20 mm-long CU showed results consistent with those reported for the larger (40 mm) GRACE-Cs (same maximum contraction ratio) [44]. However, the pressure required by the CU to reach its maximum contraction was slightly higher than the one reported for the GRACEs, as the average thickness was not scaled proportionally to the other dimensions compared to the original design. The thicker membrane (compared to a proportionally scaled one) allows withstanding higher-pressure inputs, resulting in the force exerted by the CUs to be higher than the one expected for a fully scaled-down GRACE-C design (6.8 N instead of expected 4.25 N, the latter being ¼ of the original force for a scaling factor of ½).

The results of the isotonic and isometric tests of the three muscle prototypes allowed comparing the performance achieved by both modulating the input pressure and partializing the number of active fibers (Tab.2 and fig.12).
The higher maximum contraction was achieved by the parallel prototype. However, considering the lower input pressure and the fewer actuators per fiber, the fusiform architecture has performed equivalently to the parallel one in terms of contraction. The fusiform prototype reached a maximum contraction of 28.6 mm at a pressure of 26.2 kPa, equal to 18.1 % of the length of the structure, compared to the 30.3 mm at a pressure of 28 kPa achieved by the parallel prototype, equal to 19.2 % of the length of the structure. At the same pressure input of 24 kPa, they performed similar contraction: 17.1 % for the fusiform arrangement and 17.8 % for the parallel one. The fusiform structure is able to perform, even with shorter fibers, a contraction almost equivalent to the parallel one, by offering lower passive compression resistance but at the cost of greater radial bulkiness during contraction, especially when underactuated through only some active fibers. This is due to the absence of constraints between the fibers other than the converging connectors at the fibers' ends, which facilitate their deformation without hindering the buckling phenomenon. In the parallel architecture, the constraints due to several connectors reduce the buckling phenomenon of the fibers when the structure is underactuated but also make it slightly harder to deform. Supplementary connectors can also be implemented in the other two designs if it is needed to strengthen their structures or attenuate the fibers' buckling effect during underactuated regulation at the cost of slightly reducing the contraction performance.
As expected, the bipennate architecture achieved smaller maximum contractions than the other two, having fibers consisting of three CUs and arranged at an angle of 30 degrees with respect to the tendons. The maximum contraction reached was 19.2 mm at a pressure of about 24 kPa, equal to 12.2 % of the length of the structure. In the bipennate prototype, similar to the behavior of the natural counterpart, the fibers rotate during the contraction and tend to adjust their pennation angle while pulling the tendon.
The three architecture prototypes achieved smaller contraction in percentage than the single CU. This is mainly because supporting and connective elements that do not actively participate in the contraction are present in the arrangements. Indeed, if the contraction achieved by each prototype is related to the initial length of one of its fibers instead of the length of the whole structure, it results in a contraction ratio similar to one of the single CU.

Thanks to the larger number of parallel fibers, the bipennate prototype best performed in terms of force exerted among the three arrangements. It reached a peak of 43.6 N at 26.4 kPa and around 41 N at 24 kPa, value considered to facilitate the comparison between the three prototypes. Nevertheless, the outcome force reduces partially with the deformation of some supporting elements in the structure, due to the softness of the material adopted. This effect can be lowered by enlarging the cross-section of low-resistant connecting elements in the design phase or involving stiffer materials for the whole structure. The CUs can indeed be 3D-printed with materials with a wide range of stiffness. The force attenuation due to the deformation of some elements also particularly affect the fusiform architecture performance. Here, the convergent connectors at the two ends tend to deform during the contraction, limiting the maximum force generated. The fusiform prototype achieved a maximum force of 24.8 N at 26.2 kPa and 23.3 N at 24 kPa. Considering the seven fibers in parallel composing this prototype and the force exerted by a single CU that is 6.2 N at 24 kPa, the expected force achieved by this arrangement should be 43.4 N. Thus, more than 40% of the potential force output is lost mainly due to the deformation of low-resistant supporting elements.
The parallel architecture reached a maximum pulling force close to the bipennate one through higher pressure input with fewer fibers. It achieved a maximum force of 38.8 N at a pressure of 28 kPa and 35.3 N at 24 kPa. The measured force here is almost equal to the expected one, i.e., 37.2 N at 24 kPa, differing only of about 5%. The parallel structure, indeed, does not include high-deformable elements and thus, the attenuation of the output force is small compared to the other arrangements.

The tests showed that, in all three artificial muscle arrangements, the exerted force strongly depends on the number of activated fibers and only marginally by contraction (at least in the no-load condition we tested). This is similar to the behavior of natural muscles, whose output force is regulated by the recruitment of varying numbers of muscle fibers. During isometric tests, the bipennate and parallel prototypes showed an output force almost linearly dependent on the number of fibers actuated. The bipennate prototype

achieved 33.5% of the maximum force with 33% active fibers, 67.9 with 67% active fibers, and 100% with all twelve fibers actuated. The parallel prototype reached 34.3% of the maximum force with 33% active fibers, 66.5% with 67% active fibers, and 100% with all 6 fibers actuated.

The fusiform prototype showed less linearity between the force and the number of activated fibers, with a gap between the performance of the central and the external fibers due to the force attenuation effect caused by the stretch of the converging end-connectors in the latter. Indeed, the central fiber performed higher pulling force, close to the one recorded for the stand-alone CU, than the others thanks to the more rigid end-connector. Therefore, the fusiform architecture achieved a large portion of the maximum force, equal to 26.6%, with 14% active fibers, and lower increments per fiber up to 57.3% with 57% four active fibers, 70.2% with 71% active fibers and 100% with all the seven fibers actuated.

During the isotonic tests, each of the three muscle arrangements directly reached a contraction close to the maximum when actuated only with the first group of fibers. The parallel prototype performed 71% of the maximum contraction with 33% active fibers, the bipennate 82.3% with 33% active fibers, and the fusiform 87.4% with 14% active fibers. The parallel architecture reached then the maximum contraction with 67% active fibers and no additional displacement with all six fibers actuated. The bipennate prototype reached 94.8% of the maximum contraction with 67% active fibers and the maximum displacement with all twelve fibers actuated. Finally, the fusiform prototype reached 89.2% of the maximum contraction with 57% active fibers, 93.7% with 71% active fibers, and then the maximum displacement with all the fibers actuated.

These results show that the contraction regulation based on the number of active fibers mimicking the natural one can be implemented in muscle artificial architectures, becoming particularly suitable when the number of fibers increases. In this way, it will be possible to finely regulate the force exerted while only minimally affecting the contraction displacement. This is not possible with the force-regulation based on varying the input pressure for all the fibers at the same time, which inevitably tends to regulate both the force exerted and the contraction achieved by the artificial muscle. The higher the number of fibers involved in the arrangements, the more efficient the method relying on muscle fiber recruitment will become. This method, indeed, will achieve increasingly finer and more precise force regulation as the number of fibers increases. Such high fiber densities could be obtained by reducing the dimensions of the single CU.

The tests highlighted some differences between the performances of the three muscle architectures proposed, which reflect some of the main differences between their natural counterparts. Long fibers, arranged in the same direction as the tendons, lead to the best performance in terms of contraction displacement as seen with the fusiform and parallel architectures.

Shortening the fibers and tilting them with respect to the axis of the muscle reduces muscle contraction but enables stacking them with a higher density increasing the overall force exerted. Therefore, the pennate architecture is the one able to exert the higher forces. In the design of this muscle architecture, the pennation angle is a fundamental parameter that can be exploited to suit the performances to specific needs. It can be modified to vary the balance between the contraction reduction due to the fibers' slant and the increase of their density leading to an increase in force.

The design options and the performance diversification shown here are enabled by using arrangements of multiple small units instead of a single large-size actuator to produce the contraction. By designing artificial muscles composed of sub-units hierarchically arranged in fibers is also possible to implement regulation strategies based on fiber recruitment, as

	Single CU	Fusiform (7 fibers)	Bipennate (12 fibers)	Parallel (6 Fibers)
Max Contraction	**26 %**	**18.1 %**	**12.2 %**	**19.2 %**
Contraction (24 kPa)	**22.3 %**	**17.1 %**	**12.2 %**	**17.8 %**
Max Contraction Force	**6.8 N**	**24.8 N**	**43.6 N**	**38.8 N**
Contraction Force (24 kPa)	**6.2 N**	**23.3 N**	**41 N**	**35.3 N**

Tab. 2. Performance comparison. Comparison between the maximum contractions, maximum forces, and contraction and forces at the reference pressure of 24 kPa, achieved by the three muscle architectures with all the fibers actuated during isotonic and isometric tests. As a reference, the performance of a CU is also reported. All muscles are made of 36 identical CUs arranged in different architectures.

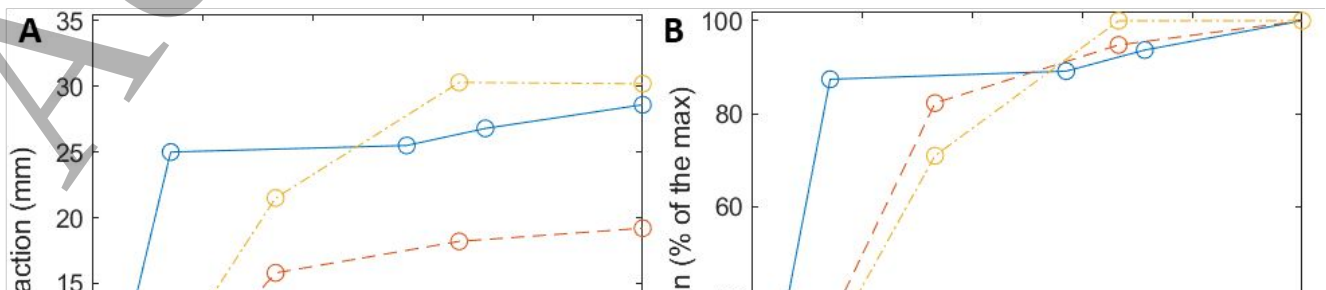

we have done here, that can improve the mimicry of the natural muscles' behavior in the artificial world.

5) Conclusion

In this paper, we demonstrate that PAMs with architectures that mimic natural muscular ones can be easily realized by single-step 3D printing of hierarchical arrangements of contractile units based on the GRACE design. The adoption of actuation systems branched in numerous units instead of a single actuator, even if not necessarily improving contraction performance, widens the design possibilities, enhances versatility, and enables the implementation of bioinspired control strategies and biomimetic movements. Here, we have developed three biomimetic muscle architectures as demonstrators: the fusiform, the parallel, and the bipennate muscles. We have carried out isotonic and isometric tests for the prototypes of the three architectures, comparing their performance and highlighting their biomimetic characteristics. This also demonstrates the potential of fully 3D-printable pneumatic actuator designs, such as that we adopted for the CUs, in realizing articulated muscle systems for the development of biomimetic machines. Unlike multifilament PAMs, consisting of McKibben thin fibers, here the single actuators play the role of the contractile units, a fibers' subunit, mimicking the functionality of the sarcomeres, which, together with the CUs tunable and 3D-printable design, increases the number of possible biomimetic arrangements. Moreover, we have also demonstrated that the biomimetic muscle architectures can in turn be 3D printed at once, without any additional assembling phases. In this way, the number of contractile units employed, their dimensions, shapes, and types of arrangements involved can all be modified by design without increasing the manufacturing effort.

We have also demonstrated a biomimetic force regulation strategy based on fiber recruitment, which allows changing the exerted force almost independently from the length contraction of the artificial muscle. In particular, for all three muscle architectures we have implemented a hybrid regulation to demonstrate that these artificial muscles allow both a conventional regulation based on the modulation of the pressure and a more biomimetic one based on fiber recruitment. The first method is efficient in systems with a limited number of degrees of freedom and becomes exponentially more complex and expensive as their number increase. The second method becomes suitable as the number of fibers increases and can be implemented to control directly the force exerted without affecting the contraction. Since it involves on/off valves instead of pressure regulators, it requires simpler and less expensive pneumatic circuits than the conventional regulation method. The two methods can also be combined if an extremely versatile regulation is required by implementing a pressure regulator for each fiber in order to regulate the system by modulating each fiber's input but at the cost of dramatically increasing the complexity of the pneumatic circuit and the overall control system.

To increase the number of fibers in the muscle architectures without changing the muscle overall dimensions, smaller CUs must be adopted, which is in principle possible with the GRACE design. The CUs minimum size is yet limited by the manufacturing techniques and materials adopted. The desktop 3D printer we used for the fabrication could have allowed further scaling down of the single CU, but this would have implied a more challenging printing of the three muscle architectures. Particularly, the biggest issue was represented by the high viscosity of the commercial resin adopted that tends to be stuck inside the actuators during printing if their size is too small and the structure does not offer enough outlets. Adopting purposely developed soft resins with lower viscosity or using different additive manufacturing technologies could solve these practical issues and enable printing muscle architectures with higher numbers of CUs and fibers, allowing the recruitment-based regulation strategy to exhibit its full potential.

While applying the recruitment-based regulation strategy, however, we have also observed undesired buckling of inactive fibers. As far as we experienced, this does not result in a loss of performance or integrity of the structure, yet it increases the overall bulkiness of the artificial muscles during compression. To avoid this, supplementary connecting elements can be additionally implemented between the CUs to constrain some secondary deformations (as we did for the parallel muscle design, which was the most affected by the issue). It is impressive to realize that nature has solved this problem by having muscle fibers embedded in a soft connective tissue, which avoids buckling without hindering contraction and force generation. Embedding the CUs in soft matrices mimicking the connective tissue of natural muscles could help addressing this issue, while also enhancing the passive storage of elastic energy during active contraction (similar to natural muscles). Nonetheless, the ratio between the stiffness of the muscle structure and the connective matrix will need to be determined carefully, since the matrix should match the artificial muscle contraction without hindering it. This will be particularly challenging. For the future, we envision the possibility of realizing PAMs with highly complex architectures enabling truly biomimetic muscular systems and, in turn, novel bioinspired machines and robots capable of smooth and articulated movements closely matching those observed in the animal world.

Funding

This work has received funding from the European Union's Horizon 2020 research and innovation program under grant agreement no. 863212 (PROBOSCIS project).

References

[1] Biewener A A 1990 Biomechanics of mammalian terrestrial locomotion *Science (80-.).* **250** 1097–103

[2] Dickinson M H, Farley C T, Full R J, Koehl M A R, Kram R and Lehman S 2000 How animals move: an integrative view *Science (80-.).* **288** 100–6

[3] Biewener, Andrew and Patek S 2018 *Animal locomotion* (Oxfort University Press)

[4] R. McNeill A 2003 *Principles of Animal Locomotion* (Princeton University Press)

[5] Biewener A A 2016 Locomotion as an emergent property of muscle contractile dynamics *J. Exp. Biol.* **219** 285–94

[6] Wilson P D 2014 *Anatomy of Muscle* vol 5 (Elsevier)

[7] Miller M S, Palmer B M, Toth M J and Warshaw D M 2017 *Muscle* (Elsevier Inc.)

[8] Carlson B M 2019 The Muscular System *Hum. Body* 111–36

[9] Firat T 2020 Architecture of muscle tissue and its adaptation to pathological conditions *Comp. Kinesiol. Hum. Body Norm. Pathol. Cond.* 101–13

[10] Macintosh B R, Gardiner P F and Mccomas A J 2006 *Skeletal muscle: form and function* (Human kinetics)

[11] Gans C and Gaunt A S 1991 Muscle architecture in relation to function *J. Biomech.* **24** 53–65

[12] Gans C and de Vree F 1987 Functional bases of fiber length and angulation in muscle *J. Morphol.* **192** 63–85

[13] Azizi E, Brainerd E L and Roberts T J 2008 Variable gearing in pennate muscles *Proc. Natl. Acad. Sci. U. S. A.* **105** 1745–50

[14] Buchthal F and Schmalbruch H 1980 Motor unit of mammalian muscle *Physiol. Rev.* **60** 90–142

[15] Winter D A 2009 *Biomechanics and motor control of human movement* (John Wiley & Sons)

[16] Delahunt S A, Pillsbury T E and Wereley N M 2016 Variable recruitment in bundles of miniature pneumatic artificial muscles *Bioinspiration and Biomimetics* **11**

[17] Bryant M, Meller M A and Garcia E 2014 Variable recruitment fluidic artificial muscles: Modeling and experiments *Smart Mater. Struct.* **23**

[18] Robinson R M, Kothera C S and Wereley N M 2015 Variable Recruitment Testing of Pneumatic Artificial Muscles for Robotic Manipulators *IEEE/ASME Trans. Mechatronics* **20** 1642–52

[19] Jenkins T E, Chapman E M and Bryant M 2016 Bio-inspired online variable recruitment control of fluidic artificial muscles *Smart Mater. Struct.* **25**

[20] Meller M, Chipka J, Volkov A, Bryant M and Garcia E 2016 Improving actuation efficiency through variable recruitment hydraulic McKibben muscles: Modeling, orderly recruitment control, and experiments *Bioinspiration and Biomimetics* **11** 1–17

[21] Higueras-Ruiz D R, Nishikawa K, Feigenbaum H and Shafer M 2022 What is an artificial muscle? A comparison of soft actuators to biological muscles *Bioinspir. Biomim.* **17** 011001

[22] Daerden F, Lefeber D, Verrelst B and Van Ham R 2001 Pleated pneumatic artificial muscles: actuators for automation and robotics *IEEE/ASME Int. Conf. Adv. Intell. Mechatronics, AIM* **2** 738–43

[23] Klute G K, Czerniecki J M and Hannaford B 2002 Artificial muscles: Actuators for biorobotic systems *Int. J. Rob. Res.* **21** 295–309

[24] Mirvakili S M and Hunter I W 2018 Artificial Muscles: Mechanisms, Applications, and Challenges *Adv. Mater.* **30** 1–28

[25] Trivedi D, Rahn C D, Kier W M and Walker I D 2008 Soft robotics: biological inspiration, state of the art, and future research *Appl. Bionics Biomech.* **5** 99–117

[26] Laschi C, Mazzolai B and Cianchetti M 2016 Soft robotics: Technologies and systems pushing the boundaries of robot abilities *Sci. Robot.* **1** 1–11

[27] Coyle S, Majidi C, LeDuc P and Hsia K J 2018 Bio-inspired soft robotics: Material selection, actuation, and design *Extrem. Mech. Lett.* **22** 51–9

[28] Miriyev A, Stack K and Lipson H 2017 Soft material for soft actuators *Nat. Commun.* **8** 1–8

[29] Miriyev A 2019 A focus on soft actuation *Actuators* **8** 74

[30] Chou C P and Hannaford B 1996 Measurement and modeling of McKibben pneumatic artificial muscles *IEEE Trans. Robot. Autom.* **12** 90–102

[31] Tondu B and Lopez P 2000 Modeling and control of McKibben artificial muscle robot actuators *Control Syst.* **20** 15–38

[32] Kurumaya S, Nabae H, Endo G and Suzumori K 2017 Design of thin McKibben muscle and multifilament structure *Sensors Actuators, A Phys.* **261** 66–74

[33] Kurumaya S, Suzumori K, Nabae H and Wakimoto S 2016 Musculoskeletal lower-limb robot driven by multifilament muscles *ROBOMECH J.* **3** 1–15

[34] Garriga-Casanovas A, Faudzi A A M, Hiramitsu T, Rodriguez Y Baena F and Suzumori K 2018 Multifilament pneumatic artificial muscles to mimic the human neck *2017 IEEE Int. Conf. Robot. Biomimetics, ROBIO 2017* **2018-Janua** 1–8

[35] Kurumaya S, Nabae H, Endo G and Suzumori K 2019 Active Textile Braided in Three Strands with Thin McKibben Muscle *Soft Robot.* **6** 250–62

[36] Faudzi A A M, Ooga J, Goto T, Takeichi M and Suzumori K 2018 Index Finger of a Human-Like Robotic Hand Using Thin Soft Muscles *IEEE Robot. Autom. Lett.* **3** 92–9

[37] Sangian D, Jeiranikhameneh A, Naficy S, Beirne S and Spinks G M 2019 Three-Dimensional Printed Braided Sleeves for Manufacturing McKibben Artificial Muscles *3D Print. Addit. Manuf.* **6** 57–62

[38] Lin Z, Shao Q, Liu X-J and Zhao H 2022 An Anthropomorphic Musculoskeletal System with Soft Joint and Multifilament Pneumatic Artificial Muscles *Adv. Intell. Syst.* **4** 2200126

[39] Higueras-Ruiz D R, Shafer M W and Feigenbaum H P 2021 Cavatappi artificial muscles from drawing, twisting, and coiling polymer tubes *Sci. Robot.* **6**

[40] Zolfagharian A, Kouzani A Z, Khoo S Y, Moghadam A A A, Gibson I and Kaynak A 2016 Evolution of 3D printed soft actuators *Sensors Actuators, A Phys.* **250** 258–72

[41] Peele B N, Wallin T J, Zhao H and Shepherd R F 2015 3D printing antagonistic systems of artificial muscle using projection stereolithography *Bioinspiration and Biomimetics* **10**

[42] Zhang C, Zhu P, Lin Y, Tang W, Jiao Z, Yang H and Zou J 2020 Fluid-driven artificial muscles: bio-design, manufacturing, sensing, control, and applications *Bio-Design Manuf.* **4** 123–45

[43] Cho K J, Koh J S, Kim S, Chu W S, Hong Y and Ahn S H 2009 Review of manufacturing processes for soft biomimetic robots *Int. J. Precis. Eng. Manuf.* **10** 171–81

[44] De Pascali C, Naselli G A, Palagi S, Scharff R B N and Mazzolai B 2022 3D-printed biomimetic artificial muscles

using soft actuators that contract and elongate *Sci. Robot.* **7** eabn4155